Supplementary Materials for:

Model-based drug-drug interaction extrapolation strategy from adults to children –risdiplam in pediatric patients with spinal muscular atrophy

Authors: Yumi Cleary[1,2], Michael Gertz[1], Paul Grimsey[3], Andreas Günther[1], Katja Heinig[1], Kayode Ogungbenro[2], Leon Aarons[2], Aleksandra Galetin[2], Heidemarie Kletzl[1]

[1]Roche Pharma Research and Early Development, Pharmaceutical Sciences, Roche Innovation Center Basel, Switzerland.

[2]Centre for Applied Pharmacokinetic Research, University of Manchester, Manchester, UK,

[3]Roche Pharma Research and Early Development, Pharmaceutical Sciences, Roche Innovation Center Welwyn, UK.

Contents

Validation. The definition of validation of PBPK models reported in the present study is an examination of the platforms and models whether they accurately predict observations from independent data (i.e., not used during model development). The independent data may have been generated for the same compound/ inhibitors (in different studies or sub-sets of populations) or other compounds with similar properties.

1. Relevant hepatic and intestinal CYP3A ontogeny functions

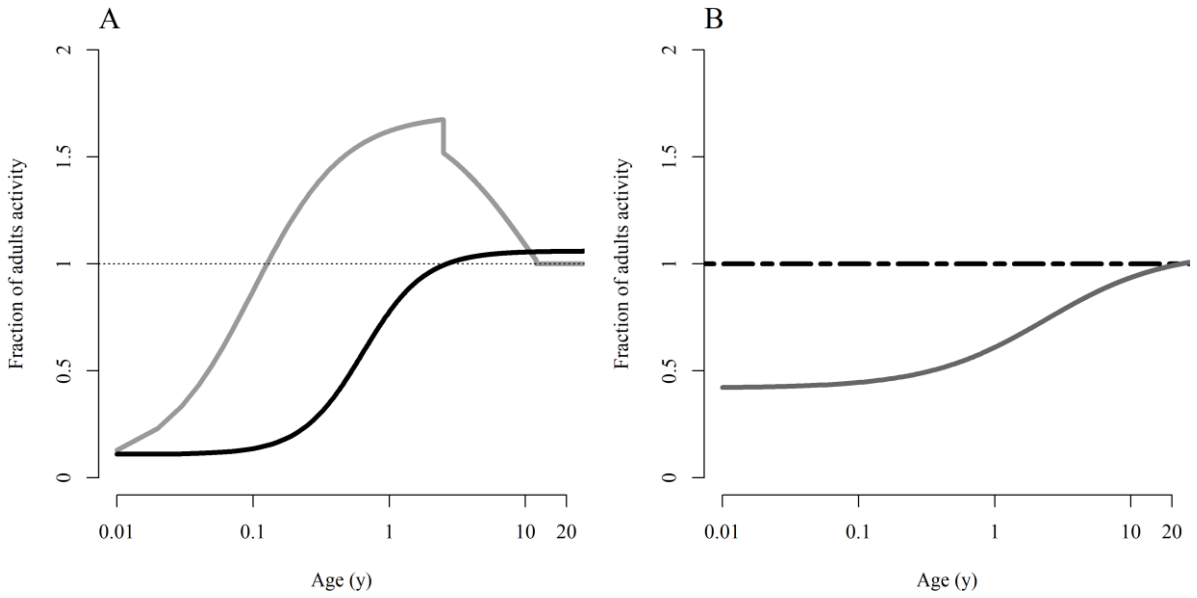

Figure S1 Hepatic and intestinal CYP3A ontogeny functions. The hepatic CYP3A ontogeny function in (A) according to Salem et al. (black solid line) and Upreti and Wahlstrom (grey solid line) and the intestinal CYP3A function in (B) according to Johnson et al (grey solid line) and full maturity from birth (black dotted line)

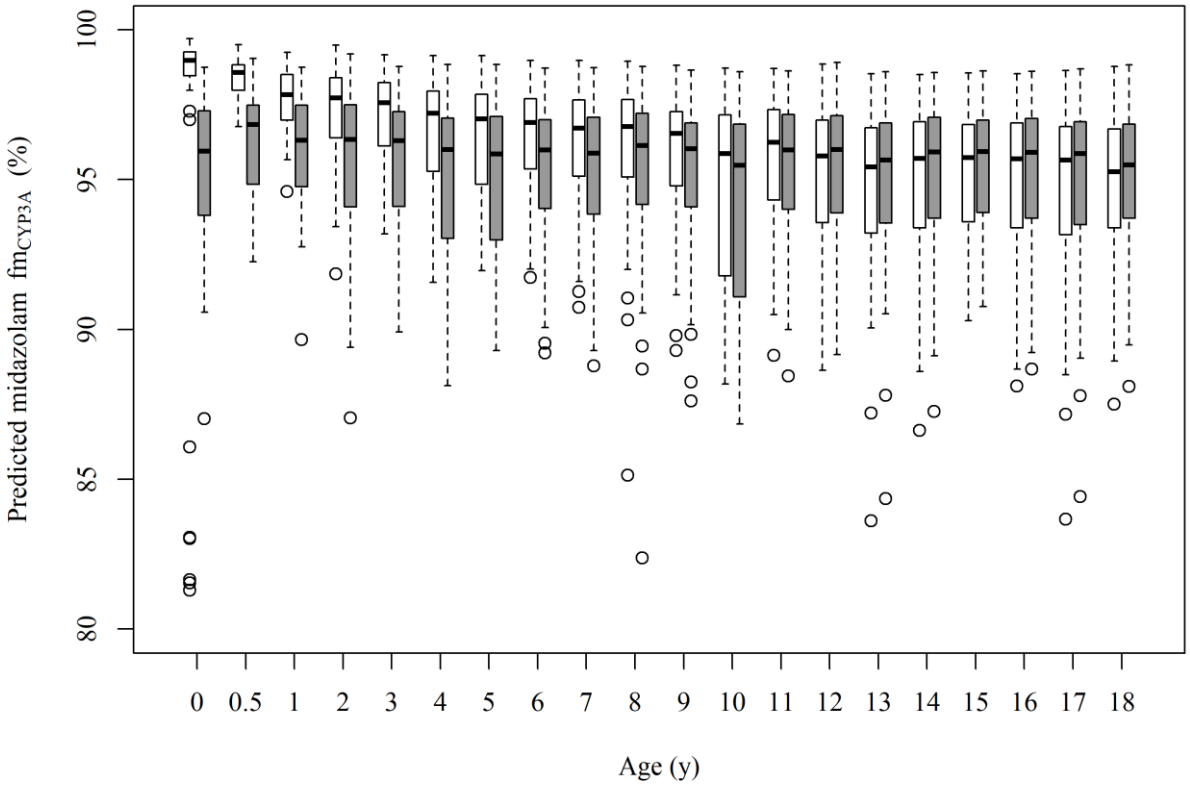

Figure S2 Predicted midazolam fm_{CYP3A} values using Upreti (white) and Salem (grey) functions for the hepatic CYP3A ontogeny.

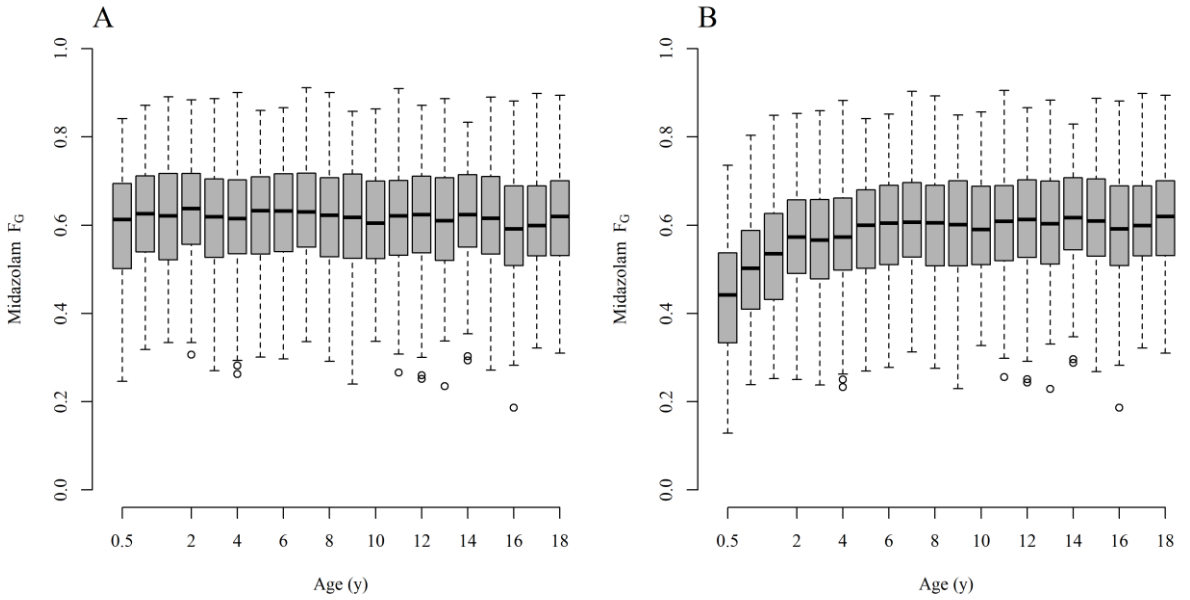

Figure S3 Predicted midazolam F_G values using Johnson function (A) and full maturity from birth (B) for the intestinal CYP3A ontogeny. The predicted intrinsic CL in the intestine (CL_{intG}) by Johnson function increases with age in parallel to Q_{Gut} (Figure S4A), resulting in the consistent F_G with age. Predicted CL_{intG} by full maturity of intestinal CYP3A from birth increases ratio of CL_{intG} over Q_{Gut} in children <2 years (Figure S4B) which leads to lower F_G than that with Johnson function.

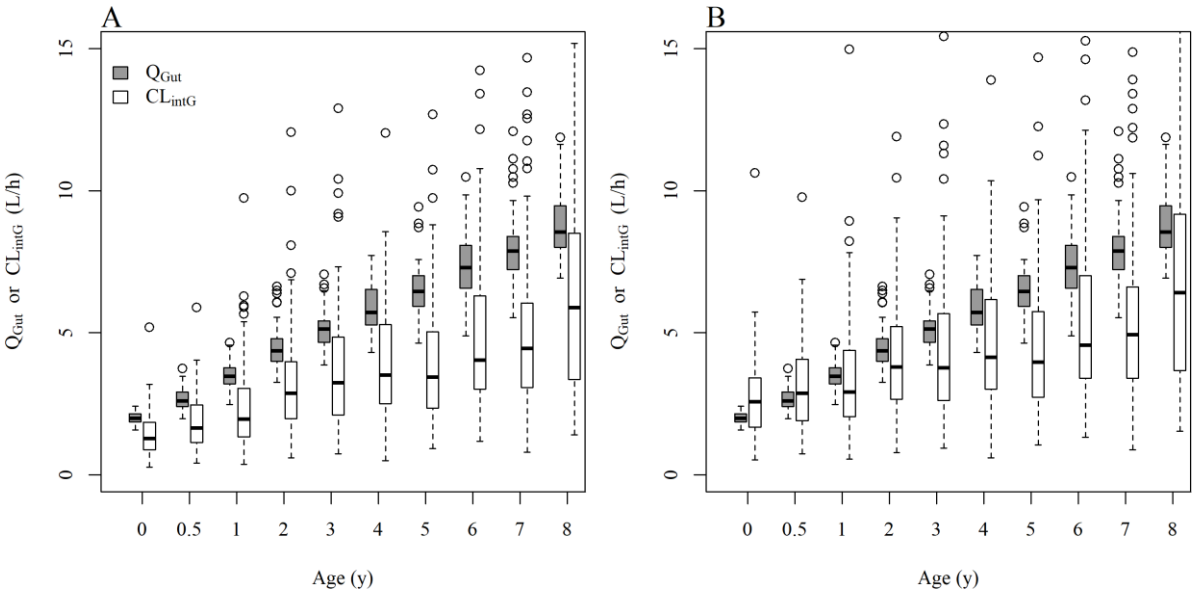

Figure S4 Predicted midazolam Q_{Gut} and CL_{intG} values using Johnson function (A) and full maturity from birth (B) for the intestinal CYP3A ontogeny.

2. Comparisons of risdiplam CL/F in pediatric SMA patients predicted by the PBPK model and *post-hoc* estimates from the population PK model

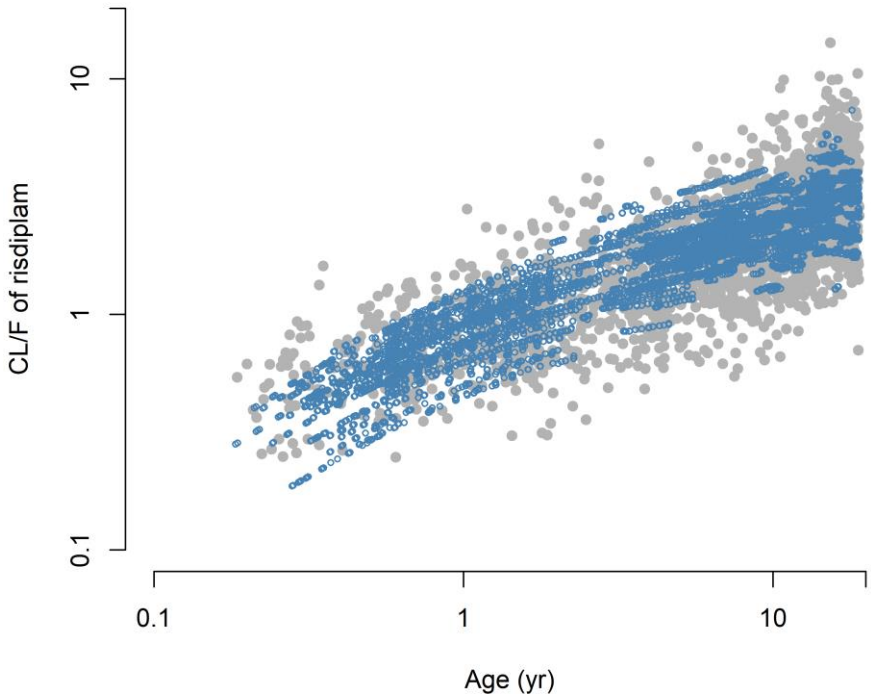

Figure S5 Comparison of risdiplam CL/F predicted by the PBPK model (grey solid circles) and *post-hoc* estimates from the PPK model (blue open circles) (1) in pediatric patients aged 2 months - 18 years. The risdiplam CL/F was estimated with good precision (relative standard error <3%) in the PPK modelling and individual *post-hoc* CL/F was estimated on sufficient information indicated by low shrinkage (5%) (1))

3. Demographic model for SMA patients

Age, body height and weight of the virtual population model in Simcyp defines physiological parameters such as organ sizes, tissue components, blood flow and renal functions (2). Therefore, an adjustment in age, body height and body weight to the actual population is considered a prerequisite of informative PBPK modelling. The demographic data of 466 SMA Type 1 – 3 patients with a total 3224 records were extracted from the population PK modelling data set mentioned above. The model of height (Equation S1) was selected according to Jolicoeur et al. (3) and the body weight model (Equation S2) was according to Simcyp version 18. Naïve pooled data were used for the analyses to estimate typical population parameters and residual error, but inter-individual variability was not estimated. The parameter estimation was performed using NONMEM version 7.4.

$$\text{Height (cm)} = \mathbf{A} \times \left\{ \mathbf{1} - \frac{\mathbf{1}}{\mathbf{1} + \left(\mathbf{t}/\mathbf{D1}\right)^{\mathbf{C1}} + \left(\mathbf{t}/\mathbf{D2}\right)^{\mathbf{C2}} + \left(\mathbf{t}/\mathbf{D3}\right)^{\mathbf{C3}}} \right\} \quad \text{Equation S1}$$

Where A is an adult height, *t* denotes the total age (age after birth plus the average duration of pregnancy (typically .75 year)), D1, D2, and D3 are three positive time-scale factors; and C1, C2, and C3 are three positive, dimensionless exponents. These parameters were estimated for male and female patients separately.

$$\text{Body weight (kg)} = W \times [(1 - e^{Age \cdot X1})] + e^{(Height \cdot X2 + X3 \cdot Age)} \quad \text{Equation S2}$$

Where the parameters *W, X1, X2* and *X3* were estimated for male and female patients separately.

3.1 The body height model

The estimated parameters for the height model are summarized in Table S1. The parameters were estimated well as indicated by the relative standard error (RSE) being less than 13% for all parameters. The residual variability (proportional error model) was estimated as 5.03% as coefficient of variation. The goodness-of-fit plots (Figure S6) show good consistency between the model predictions and observations. The model predictions capture the central tendency of the age and height relationship well across the age range in both male and female patients (Figure S7).

Table S1 Summary of estimated parameters for the body height model

Parameters	Estimate	RSE (%)
Male patients		
A: adult height (cm)	172	0.159
C1 (exponent)	0.489	3.64
C2 (exponent)	2.94	9.25
C3 (exponent)	9.08	7.5
D1 (time scale factor)	2.96	3.17
D2 (time scale factor)	9.32	1.75
D3 (time scale factor)	12.1	2.26
Female patients		
A: adult height (cm)	161	0.181
C1 (exponent)	0.54	2.19
C2 (exponent)	3.67	4.28
C3 (exponent)	13.2	12.2
D1 (time scale factor)	2.46	1.48
D2 (time scale factor)	7.89	1.20
D3 (time scale factor)	12.6	2.38
Residual error		
proportional error for all patients	0.00253 (CV = 5.03%)	1.08

RSE: relative standard error.

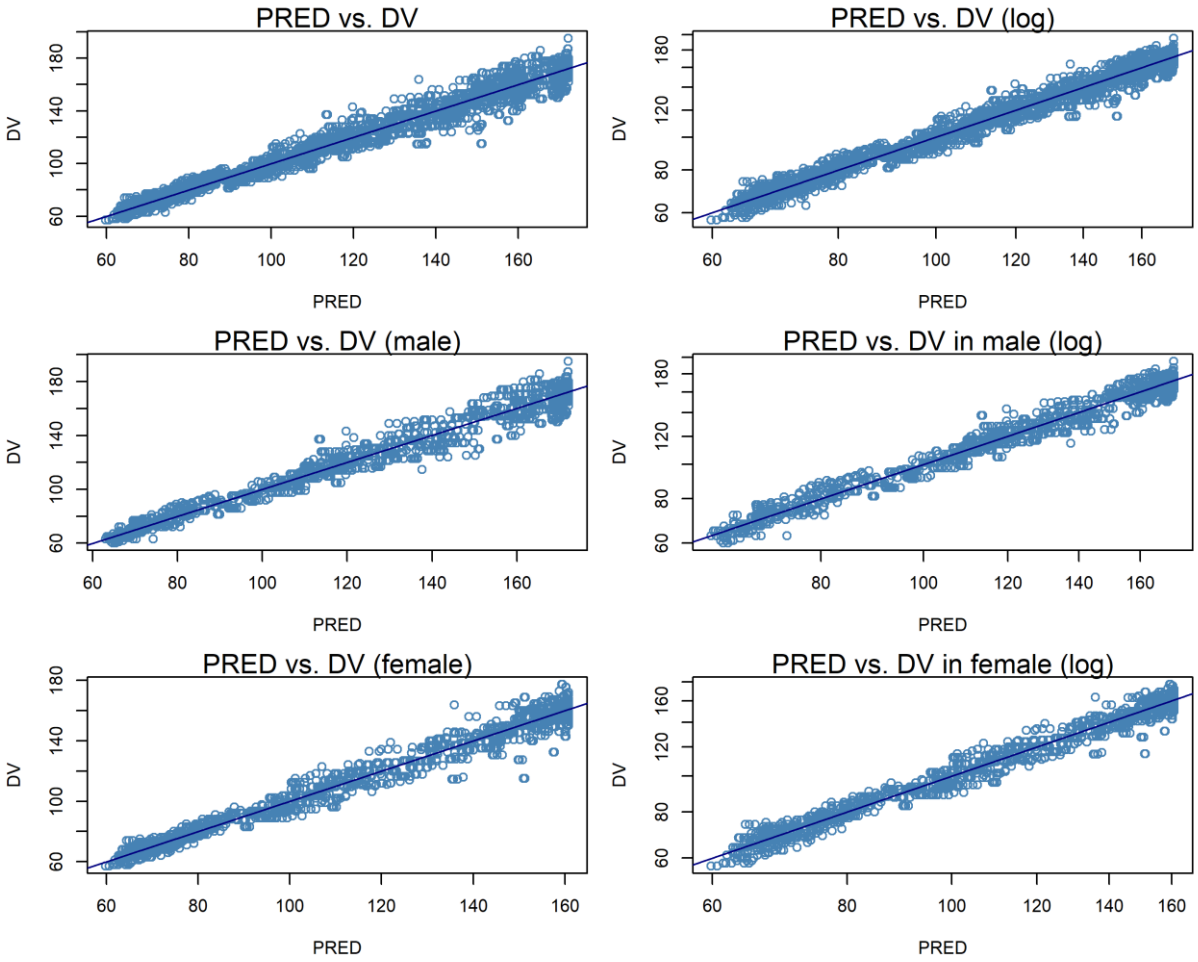

Figure S6 Goodness-of-fit plots of the height model. The solid navy lines are identity lines

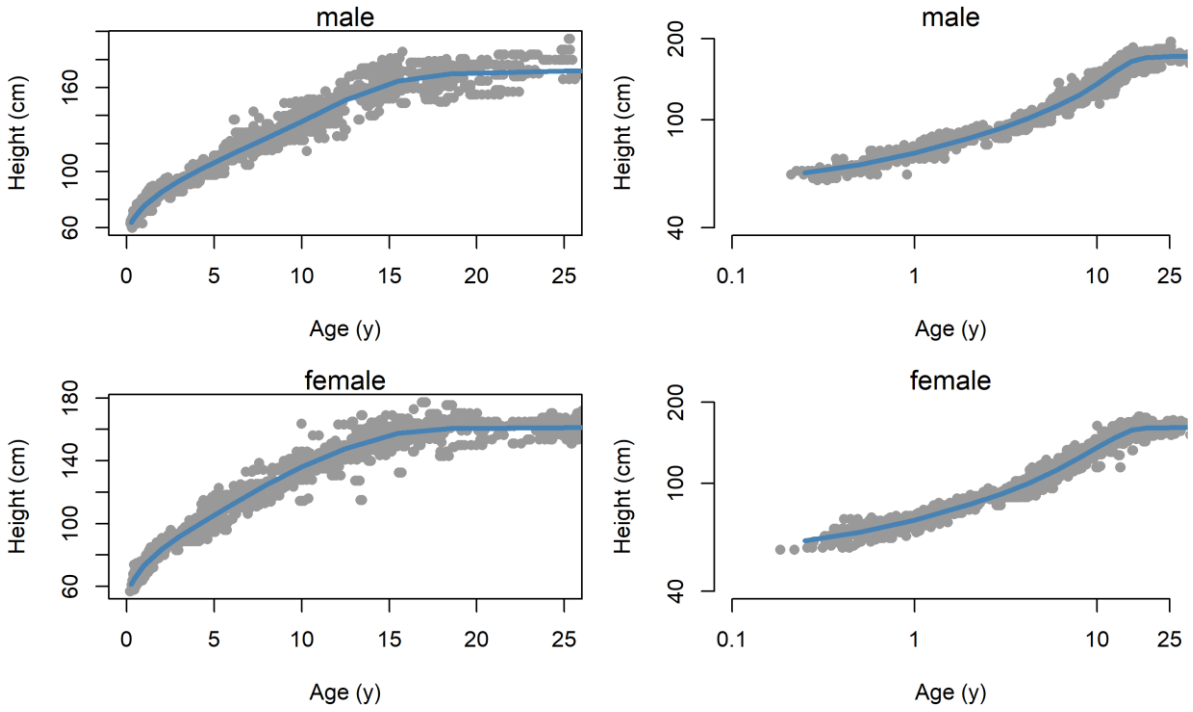

Figure S7 Comparisons of the heights between model predictions and the observed demographic data from SMA patients. The observed heights are shown in grey solid circles and the model predictions (typical growth curve) are shown with blue solid lines.

3.2 The body weight model

The estimated parameters for the body weight model are shown in Table S2. All parameters were estimated well with RSE values below 10% except for the exponent X3 for male patients where RSE was 42.9%. The goodness-of-fit plots in Figure S8 show good agreement between predicted and observed body weights. The overlay of the model prediction of the body weight on the observed body weight of the SMA patients shown in Figure S9 indicates that the model is capable of predicting the central tendency across the age range of the SMA patients.

Table S2 Summary of the parameter estimates for the body weight model

Parameters	**Estimate**	**RSE (%)**
Men		
W	3.78	2.41
X1 (exponent)	-1.40	3.81
X2 (exponent)	0.0237	0.192
X3 (exponent)	0.000552	42.9
Women		
W	3.33	2.23
X1 (exponent)	-1.7	3.9
X2 (exponent)	0.0232	0.223
X3 (exponent)	0.00655	4.79
Residual error		

< 2y	0.011 (CV = 10.5%)	2.28
2y – 10y	0.0365 (CV = 19.1%)	1.82
> 10y	0.0859 (CV = 29.3%)	1.75

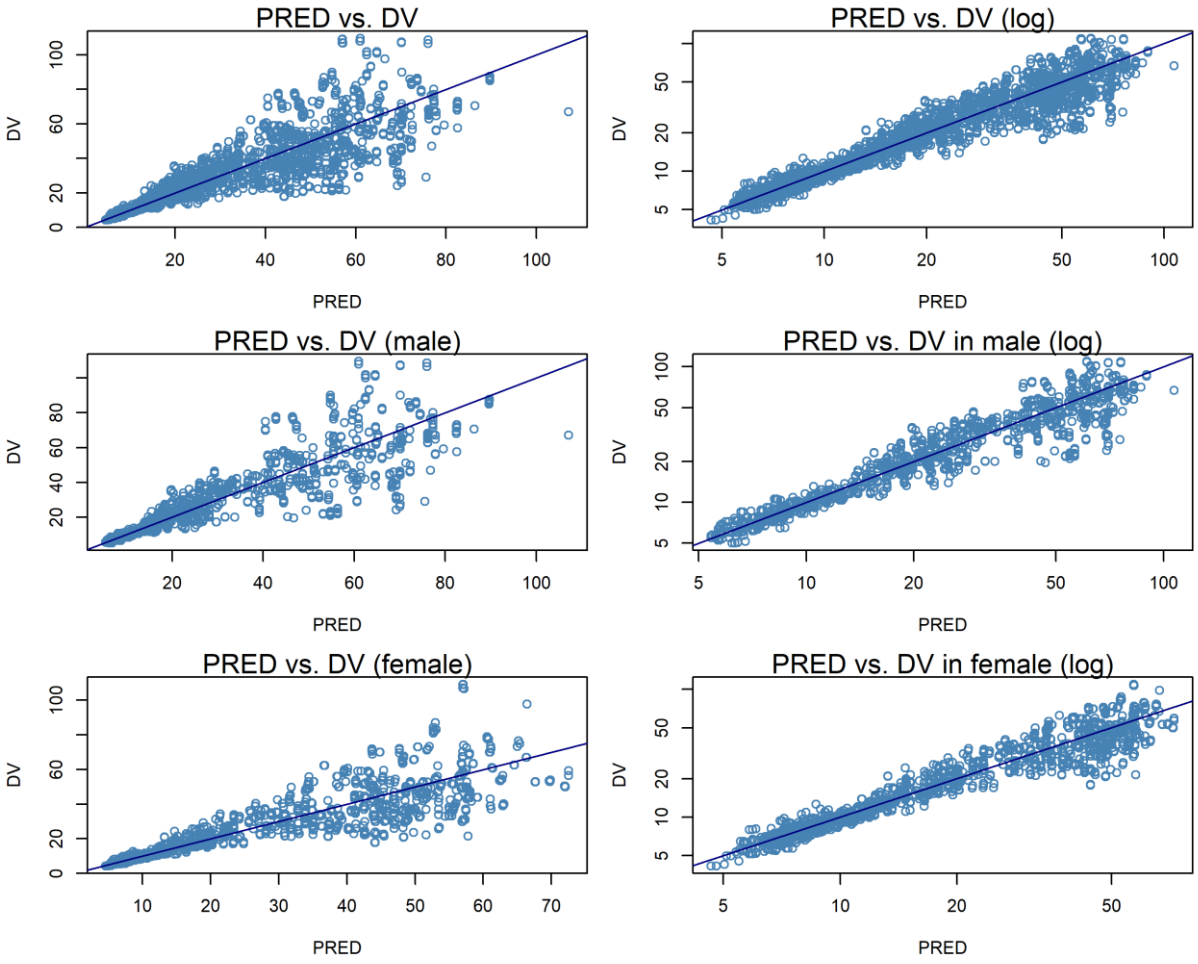

Figure S8 Goodness-of-fit plots for the body weight model. The solid navy lines are identity lines

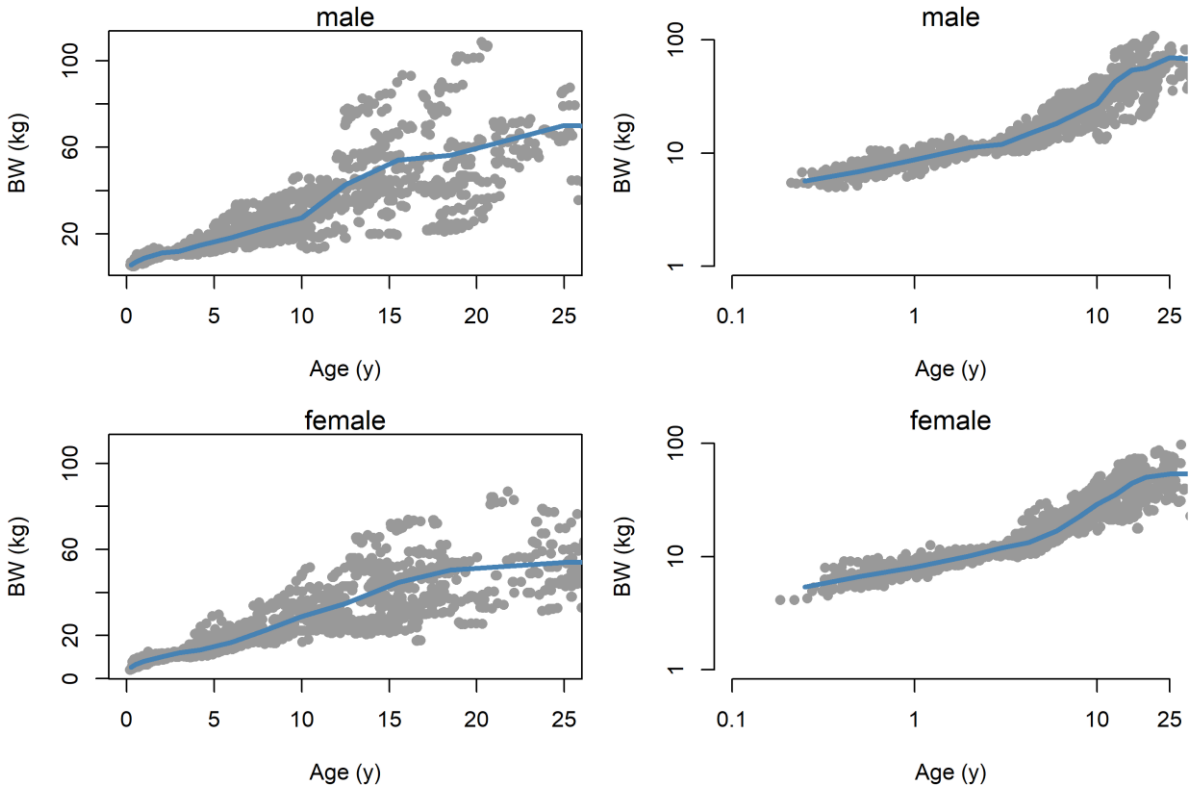

Figure S9 Comparisons of the age and body weight relationships between the model prediction (blue solid lines) and the observed in SMA patients (grey solid circles)

3.3 Implementation of the SMA demographic model in Simcyp Version 18

The body height and body weight models as well as the residual error estimated for each age group were implemented in Simcyp version 18 using Lua script (Lua.org). The comparisons of the age – body weight and – height relationships between the model predictions and the observations from the SMA patients 2 months to 18 years showed good agreement in both male and female patients (Figure S10).

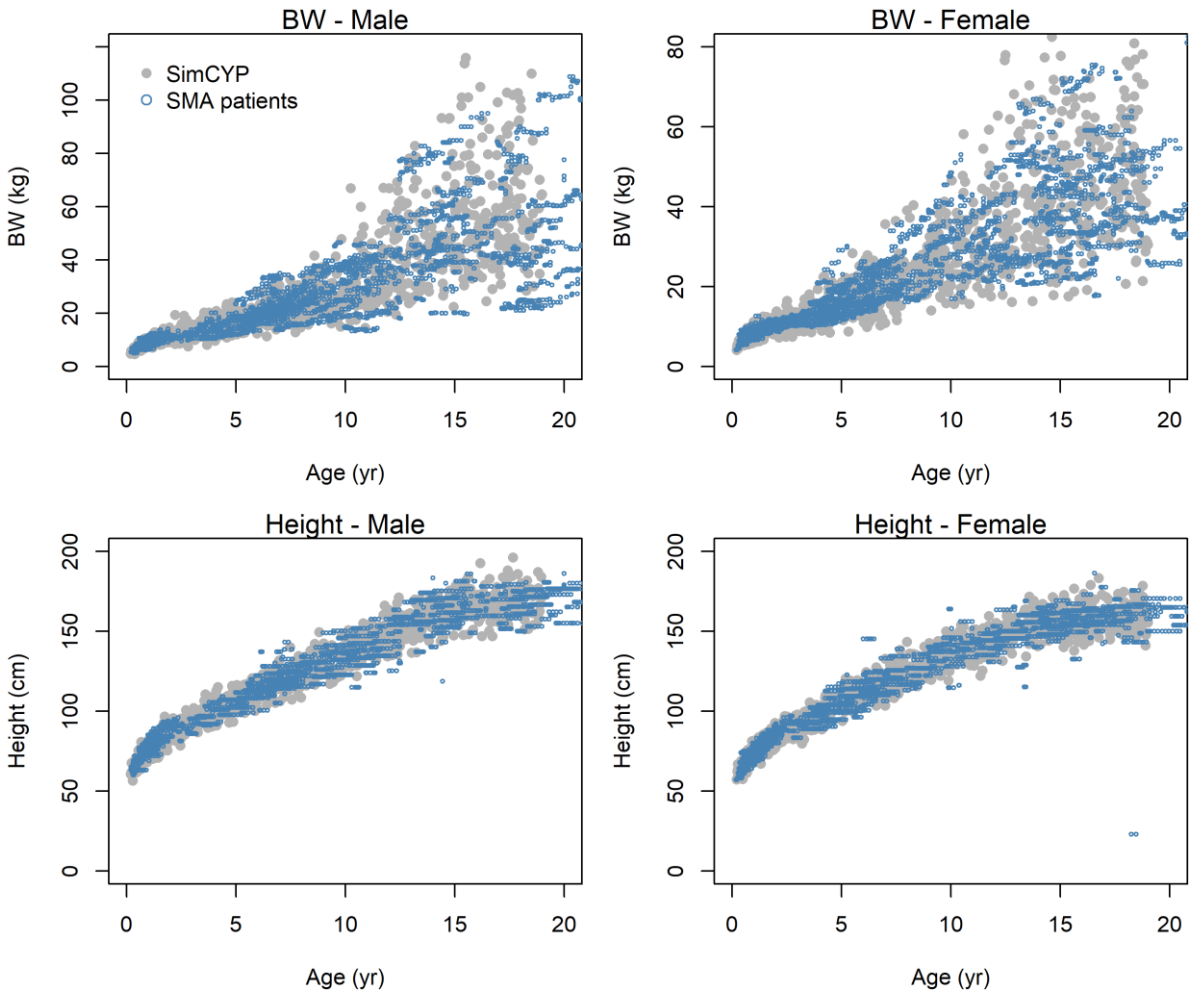

Figure S10 Comparisons of the relationship between age and body weight or height predicted by Simcyp version 18 after implementation of the growth model developed for the SMA patients. The model predicted height or body weight (grey circles) and the observations of the SMA patients between 2 months and 18 years (blue open circles) are shown for each sex.

4. Prediction of time-dependent inhibition of CYP3A

The time-dependent inhibition (TDI) of CYP3A as a function of unbound risdiplam concentrations in the liver and intestine was predicted according to Equation S3. Since risdiplam exposure after therapeutic doses are much lower than the K_I, Equation S3 is simplified to Equation S4 which is a proportional inhibition condition. The *in vivo* TDI parameters of risdiplam was estimated by optimizing k_{inact} using the clinical DDI study data because only the ratio of k_{inact} and K_I could be identified and therefore decreasing k_{inact} or increasing K_I would have produced the same outcome.

$$\frac{dE}{dt} = \frac{k_{inact} \times I_t}{K_I + I_t} \times E_t \quad \text{Equation S3}$$

$$\frac{dE}{dt} = \frac{k_{inact} \times I_t}{K_I} \times E_t \quad \text{Equation S4}$$

where E_t is amount of active CYP3A enzyme in the liver or intestine at time *t*, k_{inact} is a rate constant of enzyme inactivation, K_I is a inhibition potency parameter and I_t represents the unbound inhibitor concentrations in the liver and intestine at time *t*. The predicted unbound fractions for risdiplam and M1 were 0.82 and 0.95, respectively (4). The default degradation rate constant (k_{deg}) of 0.019 h^{-1} and 0.03 h^{-1} for the hepatic and intestinal CYP3A of Simcyp version 18, respectively were used.

5. Clinical DDI study with midazolam in healthy adults

The study subjects included 35 male and female individuals aged 18 – 55 years with a body mass index between 18.0 and 32.0 kg/m^2. Blood samples for risdiplam PK assessment were collected at pre-dose and at 0.5, 1, 2, 3, 4, 5, 6, 8, 10, 12 and 24 h post dose at the first and 14th doses of risdiplam. Additionally, pre-dose samples were taken on Days 3 to 13 and at 36, 48, 96, and 144 h after the last dose on Day 14. Midazolam PK samples were collected at pre-dose, 0.5, 1, 1.5, 2, 3, 4, 6, 8, 10, 12, and 24 h post-dose. All subjects were fasted when intensive blood samples for risdiplam and midazolam were collected for PK assessments. The second dose of midazolam (on Day 14) was given 1 h after administration of risdiplam.

5.1 Plasma concentrations and PK parameters of risdiplam and M1

Plasma concentrations of risdiplam and its metabolite M1 were measured by a validated LC-MS/MS method with the quantification limit of 0.25 ng/mL. Calibration range was up to 250 ng/mL using 40 µL plasma aliquots. Accuracy (%RE) and precision (%CV) for risdiplam ranged from 0% to 2.4% and from 2.1% to 8.2%, respectively. For M1, accuracy and precision ranged from -1.6% to 2.4% and from 2.4% to 4.4%, respectively.

The PBPK model predictions of plasma concentration time profiles after 5 and 8 mg once daily for 14 days in healthy adults were compared with the observations in Figure S11. The summary of PK parameters of M1 and metabolite to parent ratios is shown in Table S3.

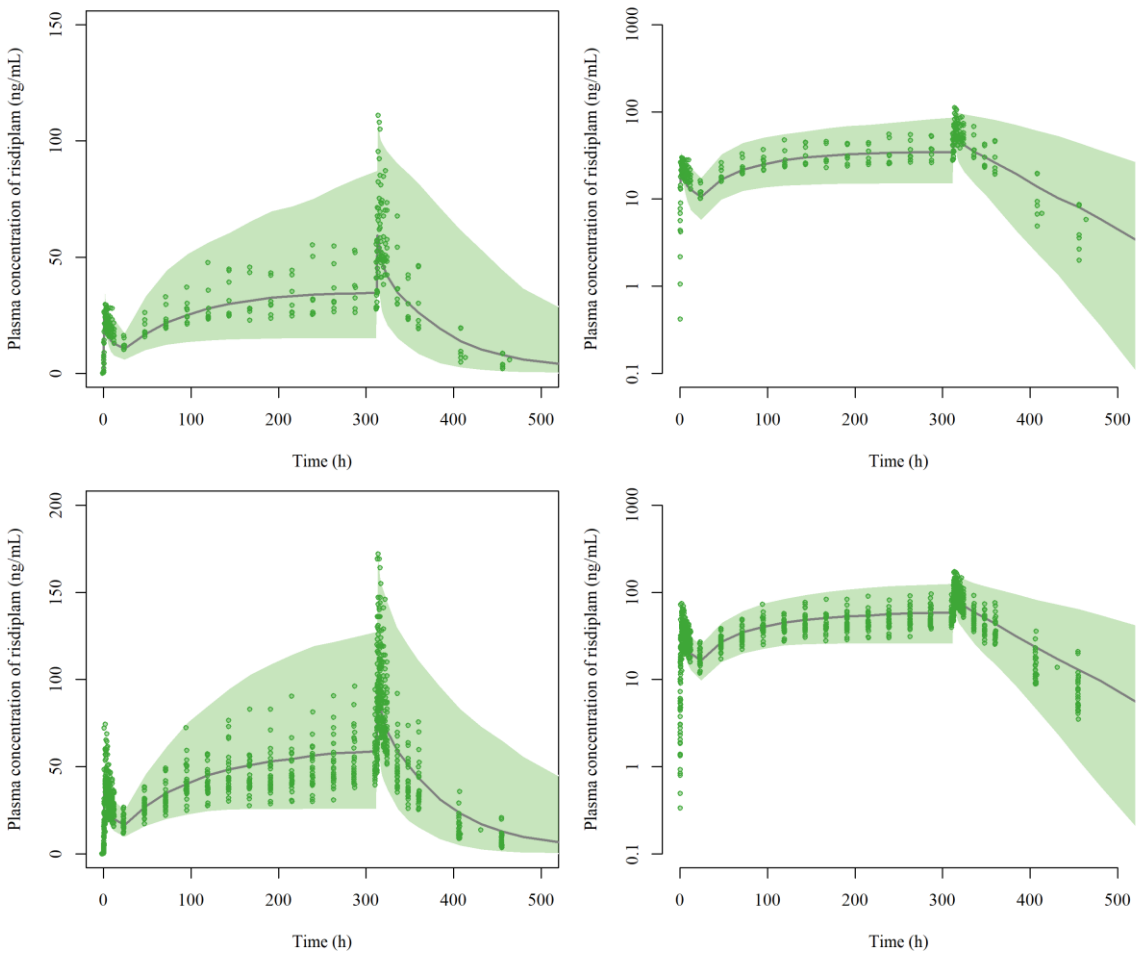

Figure S11 Simulated and observed risdiplam plasma concentration – time profiles after 5 (top) or 8 mg (bottom) once daily oral administrations for 14 days. Observations (circles), median (solid line) and 90% prediction interval (shaded area) of risdiplam are shown.

Table S3 Summary of the observed PK parameters of M1 after 5 or 8 mg once daily of risdiplam for 14 days

Dose	Parameters	Unit	Value[a]
5 mg	C_{max}	ng/mL	19.1 (20.7%)
(n=8)	$AUC_{0\text{-}24h}$	h·ng/mL	349 (23.8%)
	MR_{Cmax}	-	0.233 (8.9%)
	$MR_{AUC0\text{-}24h}$	-	0.289 (9.9%)
8 mg	C_{max}	ng/mL	30.5 (32.5%)
(n=27)	$AUC_{0\text{-}24h}$	h·ng/mL	504 (31.6%)
	MR_{Cmax}	-	0.260 (19.9%)
	$MR_{AUC0\text{-}24h}$	-	0.303 (17.5%)

[a]geometric mean (CV%). MR: metabolite (M1) to parent ratio.

5.2 Plasma concentrations and PK parameters of midazolam and 1-hydroxymidazolam

Plasma concentrations of midazolam and its metabolite 1-hydroxymidazolam were determined by a validated LC-MS/MS method with the quantification limit of 0.1 ng/mL and the calibration range

of up to 100 ng/mL using 20 µL plasma aliquots. Accuracy (%RE) and precision (%CV) for midazolam ranged from -8.3% to -1.3% and from 2.3 to 19.1%, respectively. For 1-hydroxymidazolam, accuracy and precision ranged from -1.8% to 3.4% and from 2.5% to 19.0%, respectively.

PK parameters of M1 were determined for the quantified plasma concentrations of M1 in the study as summarized in **Table S4**.

Table S4 Summary of the observed PK parameters of 1-hydroxymidazolam

Analyte	Day	Parameters	Unit	Value[a]
1'OH-midazolam	1(n=27)	C_{max}	ng/mL	3.18 (45.2%)
		AUC_{inf}[b]	h·ng/mL	8.66 (34.1%)
		AUC_{last}	h·ng/mL	7.75 (39.8%)
	15 (n=26)	C_{max}	ng/mL	4.10 (38.3%)
		C_{max} ratio[c]	-	1.27 [1.14-1.41]
		AUC_{inf}	h·ng/mL	9.41 (33.6%)
		AUC_{inf} ratio[c,d]	-	1.12 [0.99 – 1.27]
		AUC_{last}	h·ng/mL	9.43 (34.4%)
		AUC_{last} ratio[c]	-	1.20 [1.11 – 1.30]

[a]geometric mean (CV%), [b]n=17, [c]geometric least squares means (% difference from the corresponding observed values) are presented. [d]n=15. Numbers in the square brackets are 90% confidence intervals.

6. Population PK analysis of midazolam

A population pharmacokinetic (PK) analysis of midazolam was performed with 523 plasma concentrations of midazolam collected from 27 male and female healthy subjects. NONMEM version 7.4.3 (ICON Clinical Research LLC, Gaithersburg, MD, USA) and R version 3.6.1 with RStudio (version 1.2.1335) were used for the analysis. Perl-speaks-NONMEM (PsN) version 4.9.3 was used for model diagnostics. A structural PK model consisting of 8 transit compartments for absorption linked to a linear 2-compartmental disposition model adequately described midazolam plasma concentrations-time profiles. Inter-individual variability was estimated for the transit rate constant (ktr), apparent clearance (CL/F), central and peripheral volume of distributions (Vc/F and Vp/F, respectively) and inter-compartmental clearance (Q/F). A proportional error model was used to describe the residual error. A common random effects parameter for inter-occasion variability was considered for all 5 structural parameters. The effect of multiple dosing of risdiplam on midazolam PK was examined by estimating fractional changes in CL/F and relative bioavailability (F_{rel}) for Period 2, administration of midazolam in the presence of risdiplam, compared to Period 1, administration of midazolam alone.

The results of the PPK analysis are summarized in Table S5. Relative bioavailability, F_{rel} increased by 11% in the presence of risdiplam and its inclusion significantly reduced the objective function value (OFV, Wald-test). In contrast, the change in OFV did not reach statistical significance when risdiplam treatment was included as a covariate for CL/F alone or in combination with F_{rel}. The model with risdiplam effect on F_{rel} was evaluated by bootstrap analysis (200 replicates), goodness-of-fit (GOF) plots and visual predictive checks. The parameter estimates and median of the bootstrap analyses, based on 76.5% converged runs, are consistent as shown in Table S5. The 95% confidence intervals (CI) are mostly consistent except for Vp/F where a high degree of uncertainty was indicated by the estimate from the covariance matrix. The GOF (Figure S12) shows good consistency between observations and predictions, and distribution of conditional weighted residual (CWRES) was considered generally acceptable. The visual predictive check (Figure S13) indicates that the model predicts both central tendency as well as variability.

The population analysis suggests that the risdiplam effect on midazolam PK is minor and likely linked to the first pass effect. The estimated 11% increase in F_{rel} in the presence of risdiplam supports the k_{inact} optimization based on AUC_{last} fold increase of 11% determined by the non-compartmental analysis. There was no clear relationship between risdiplam $AUC_{0\text{-}24h}$ or C_{max} in Part 2 with the ratios of midazolam AUC_{last} or individual estimates of CL/F in the presence to the absence of risdiplam as shown in Figure S14. Lack of clinical relevance and concentration dependency in the change of midazolam PK implies that estimation of the *in vivo* k_{inact} by population PK modelling analysis would be unidentifiable and that local, intestinal concentrations are more likely to have caused the minor DDI observed. This is consistent with the PBPK analysis which predicted a 20% reduction in CYP3A contents in the small intestine compared to 3% reduction in the liver, likely due to the higher risdiplam concentrations in the intestine during the absorption phase. Approximately 60% of the midazolam PK samples collected at 24h post dose were below the quantification limit (BLQ) from both Parts 1 and 2. The parameter estimation was repeated with the M3 method (5) to take these BLQ data into consideration. The population estimates and bootstrap analysis, resampled 200 times, resulted in similar estimates including the F_{rel}, suggesting that the PK samples collected before 24h contained sufficient information to detect risdiplam effect on midazolam PK.

Table S5 Summary of parameter estimates of the population PK analysis for midazolam PK with and without concomitant risdiplam administration

Parameters	**Estimates**	**Covariance**		**Bootstrap***	
		RSE (%)	**95% CI (SE)**	**Median**	**95% CI**
PPK model of midazolam					
ktr (h^{-1})	19.4	10.4	15.5-23.4	19.4	17.0-22.0
CL/F (L/h)	90.9	9.14	74.6-107	89.3	79.6-107
Vc/F (L)	185	14.0	134-235	183	154-217
Q/F (L/h)	51.2	7.68	43.5-58.9	50.7	43.0-60.6
Vp/F (L)	229	87.9	-166-624	229	175-298
AGE-CL/F	-1.14	39.8	-2.03–0.251	-1.19	(-1.72)-(-0.766)
F_{rel}	1.11	2.81	1.05-1.17	1.10	1.02-1.23
IIV-ktr (CV%)	0.0546 (23.4)	40.3	0.0115-0.0977	0.0465	0.0179-0.106
IIV-CL/F (CV%)	0.0845 (29.1)	37.3	0.0227-0.146	0.0771	0.0214-0.138
IIV-Vc/F (CV%)	0.1280 (35.8)	32.2	0.0472-0.208	0.118	0.0468-0.205
IIV-Q/F (CV%)	0.0896 (30.0)	38.2	0.0226-0.157	0.0861	0.0292-0.181
IIV-Vp/F (CV%)	0.2060 (45.4)	29.0	0.089-0.323	0.198	0.0544-0.322
Inter-occasion variability	0.0263 (16.2)	27.3	0.0122-0.0403	0.0256	0.0151-0.0437
Proportional residual error (%)	10.4	10.3	8.28-12.5	10.3	8.75-11.9
Investigation of risdiplam effect		**Estimates**		**ΔOFV**	

Risdiplam effect on F_{rel}	+11%	-12.5
Risdiplam effect on CL/F	-8.0%	-3.02
Risdiplam effect on F_{rel} and CL/F	F_{rel} = +20%, CL/F = +4.7%	+9.42

*Based on 76.5% successfully minimized analyses of 200 replicates. IIV: inter-individual variability estimates as variance (estimated CV%).

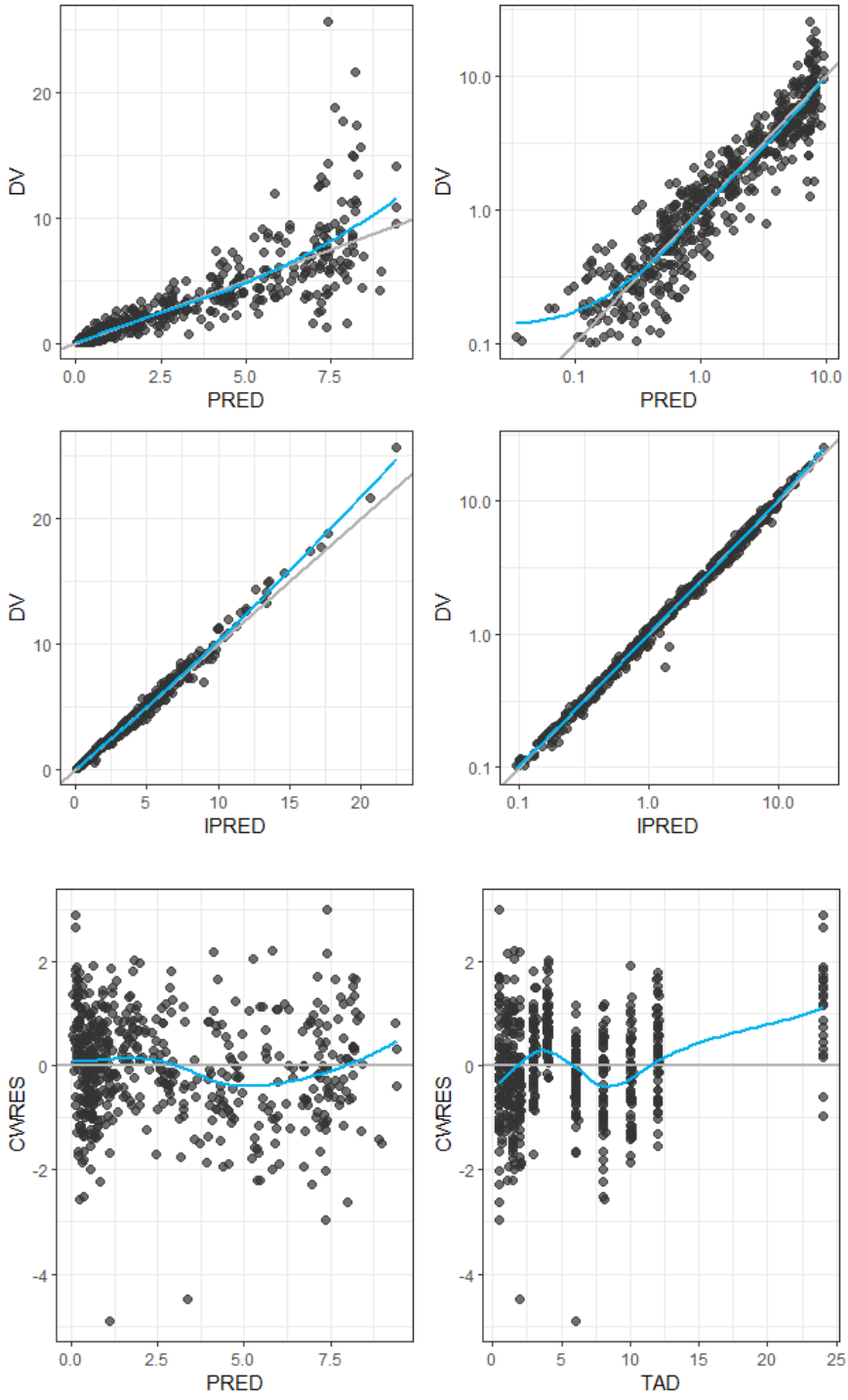

Figure S12 Goodness-of-fit plots of the midazolam population PK model

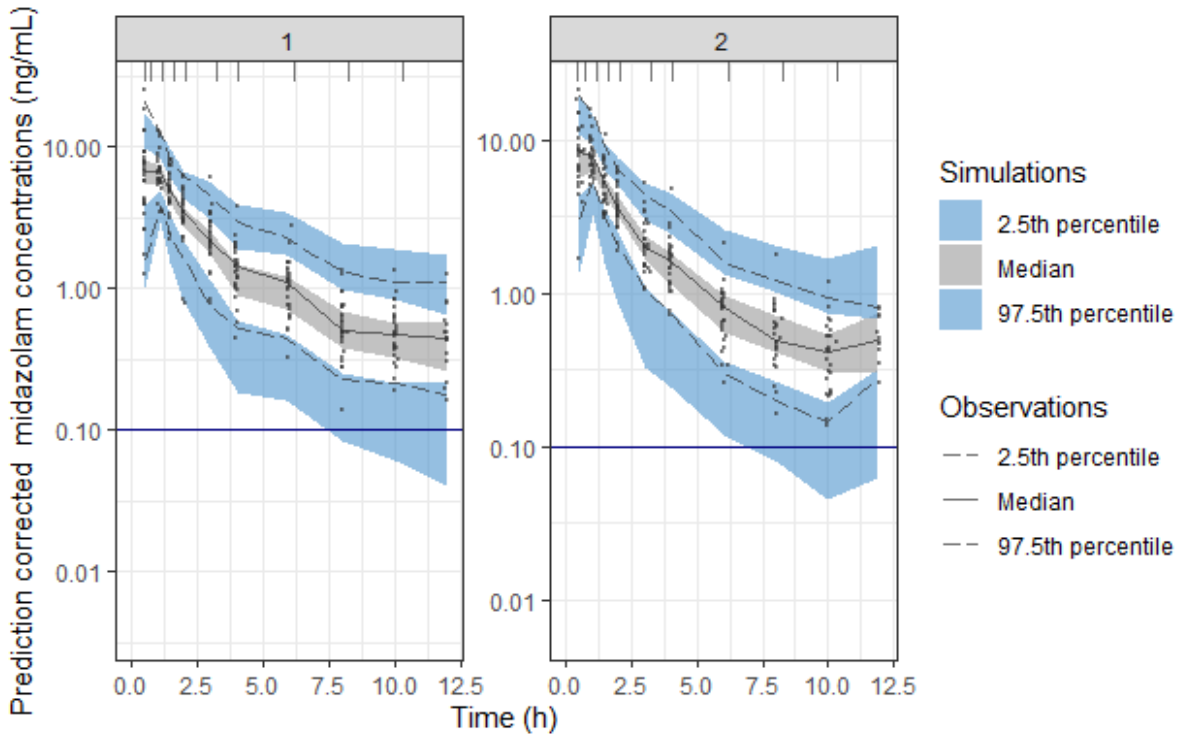

Figure S13 Visual predictive check of the population PK model of midazolam without (left) and with (right) risdiplam 8 mg QD. The solid navy line indicates quantification limit of 0.1 ng/mL.

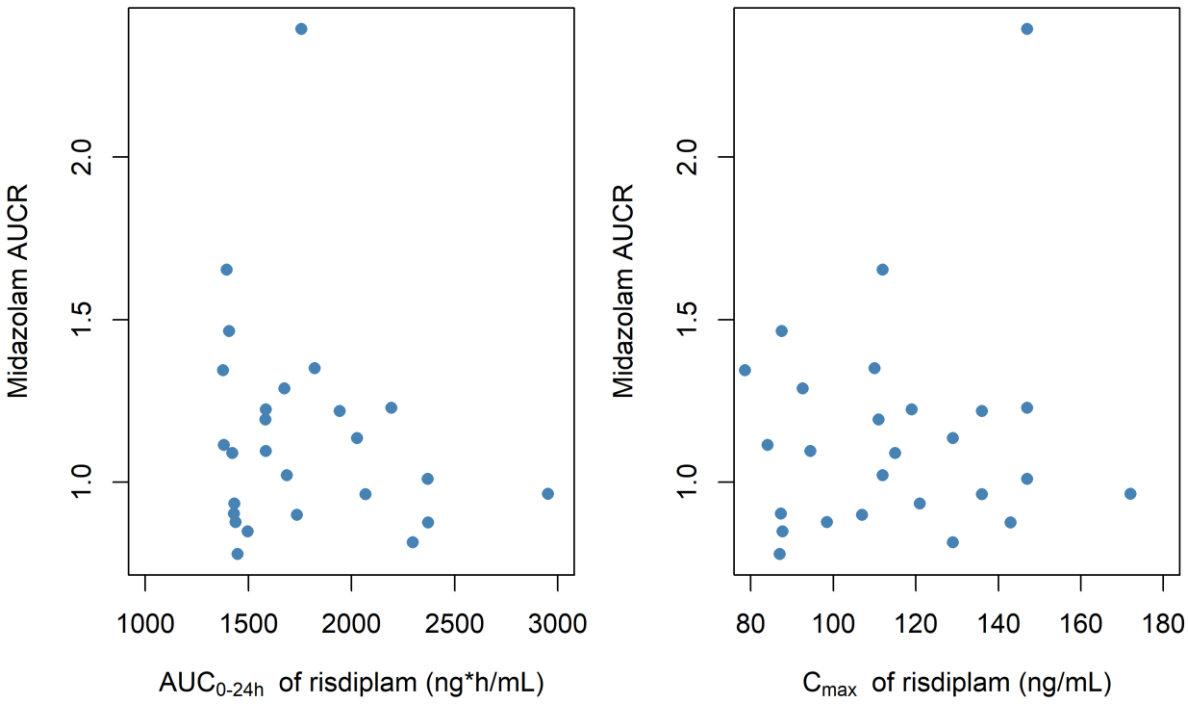

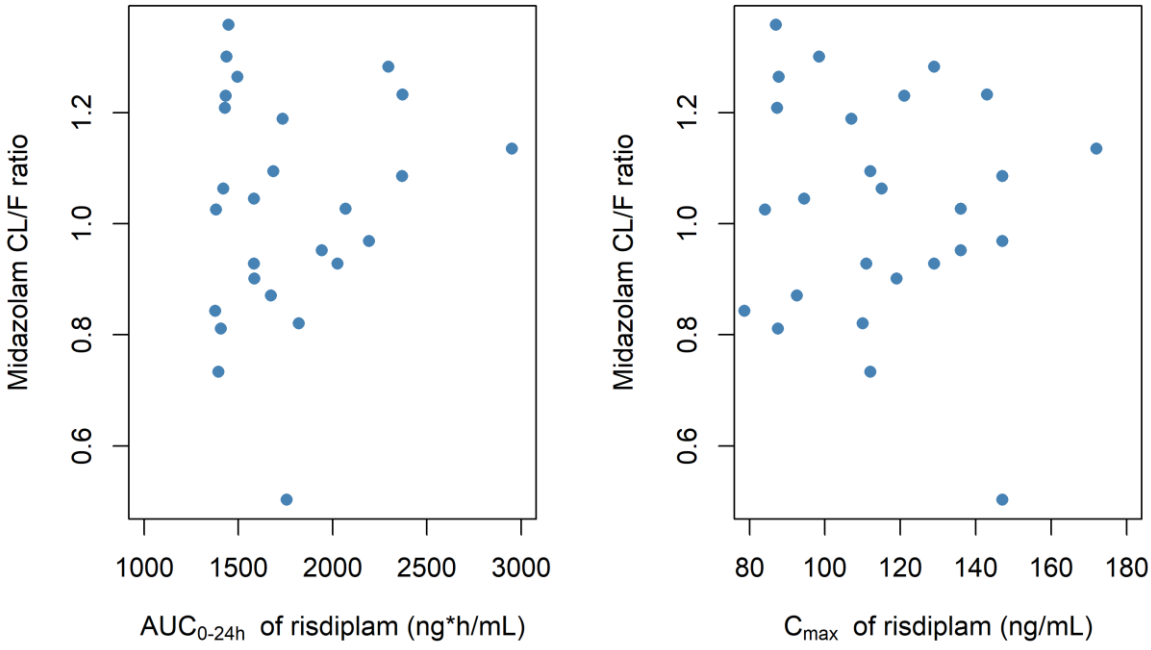

Figure S14 Relationship between ratios of midazolam parameters (AUC and CL/F) and risdiplam exposure parameters ($AUC_{0\text{-}24h}$ and C_{max}) of Part 2.

7. Validation of midazolam PBPK model in pediatric population

The default midazolam PBPK model supplied in Simcyp version 18 was used in the current investigation. The model for healthy adults was verified by the midazolam plasma concentration time profiles as well as PK parameters of these 27 healthy adults who participated in the clinical DDI trial with risdiplam (Figure 2B and Table 2). The model for pediatric population was validated using published data from clinical studies in children. The evaluation focused on whether the model can accurately predict: 1) oral and systemic midazolam CL, 2) plasma concentration time profiles of midazolam after oral and i.v. administration and 3) oral bioavailability. While intestinal CYP3A ontogeny is considered important information for DDI extrapolation for risdiplam, F_G could not be directly observed. Therefore, F_G and intestinal CYP3A ontogeny were indirectly examined by evaluation of systemic CL, hepatic availability (F_H) and oral bioavailability ($F=F_A \cdot F_H \cdot F_G$). Almost complete absorption of midazolam after oral administration ($F_A>0.9$) was assumed since permeability is high and the drug is administered as a solution. The hepatic CYP3A7 ontogeny was not considered since the metabolic specificity for midazolam is considerably lower compared to CYP3A4/5 (6).

7.1 Evaluation of oral and systemic CL of midazolam in pediatric population

As summarized in Table S6, three studies indicate that the midazolam model and the pediatric module incorporating age-dependent physiology including hepatic and intestinal CYP3A ontogeny functions of Simcyp are capable to predict oral and systemic midazolam CL in pediatric population from neonates to 18 years old children.

Table S6 Summary of literature including evaluations of the midazolam PBPK model of Simcyp in pediatric populations

Authors	Age	Midazolam model evaluation
Salem et al. (7)	1 day – 17 years	• Hepatic CYP3A ontogeny function was developed using midazolam CL values determined after i.v. administration in pediatric population reported in 15 studies (neonates= 6, infants = 5, children=9 and adolescents=4 studies). Approximately 300 pediatric subjects were included in the assessment. • Using the default midazolam model supplied in Simcyp version 12 and the developed hepatic CYP3A ontogeny function, the authors

		demonstrated good prediction of midazolam CL across the age with weighted mean fold errors of 1.40.
Upreti and Wahlstrom (8)	Neonates – 18 years	• Hepatic CYP3A ontogeny function was developed using *in vitro* (abundance of the enzyme) and *in vivo* (sufentanil PK data in pediatric and adult subjects after i.v. administration) data. • The authors simulated midazolam PK after oral and i.v. administration in pediatric population using the default Simcyp midazolam model of Version 13, with implementation of the developed *in vitro* and *in vivo* CYP3A ontogeny models. The oral and systemic midazolam CL of pediatric population were accurately predicted when *in vivo* CYP3A ontogeny model was applied.
Smits et al. (9)	Neonates	• Default midazolam model of Simcyp version 18 with modified volume of distribution was used to simulate steady-state concentrations in neonates after i.v. infusion of midazolam. • The simulated steady-state concentration of midazolam was within 20% deviation from the observations in 19 neonates reported by Mulla et al. (10).

7.2 Plasma concentration time profiles of midazolam in pediatric population

Two suitable population PK models of midazolam were identified with which the prediction by PBPK modeling could be compared. Burtin et al. (11) reported a population PK model developed on data after i.v. dosing (combination of i.v. bolus and infusion) in neonates (0 to 10 days, n = 187). A population PK model of midazolam after i.v. and oral dosing was reported by van Groen et al. (2020) (12) in children aged between 0.3 weeks to 5.3 years (n = 46, with the majority of children being less than 6 months old). Simulations of plasma concentration time profiles of midazolam after an i.v. bolus dose of 0.15 mg/kg or oral dose of 0.5 mg/kg were performed for a virtual population of 1000 children with matched age and body weight distribution for each study using the population PK and PBPK models. Simulations with PBPK model was repeated with Salem and Upreti hepatic CYP3A ontogeny function, and Johnson function was used for the intestinal CYP3A ontogeny for the simulation after oral midazolam administration. NONMEM version 7.4 was used for the simulations with the population PK models and Simcyp version 18 was used for PBPK model simulations.

The median of simulated plasma concentrations by the PBPK model showed good consistency with that by the population PK model according to Burtin et al. (11) for both Upreti and Salem hepatic CYP3A ontogeny functions (Figure S15). The PBPK model predicted inter-individual variability of these neonates was generally consistent with that of the population PK model.

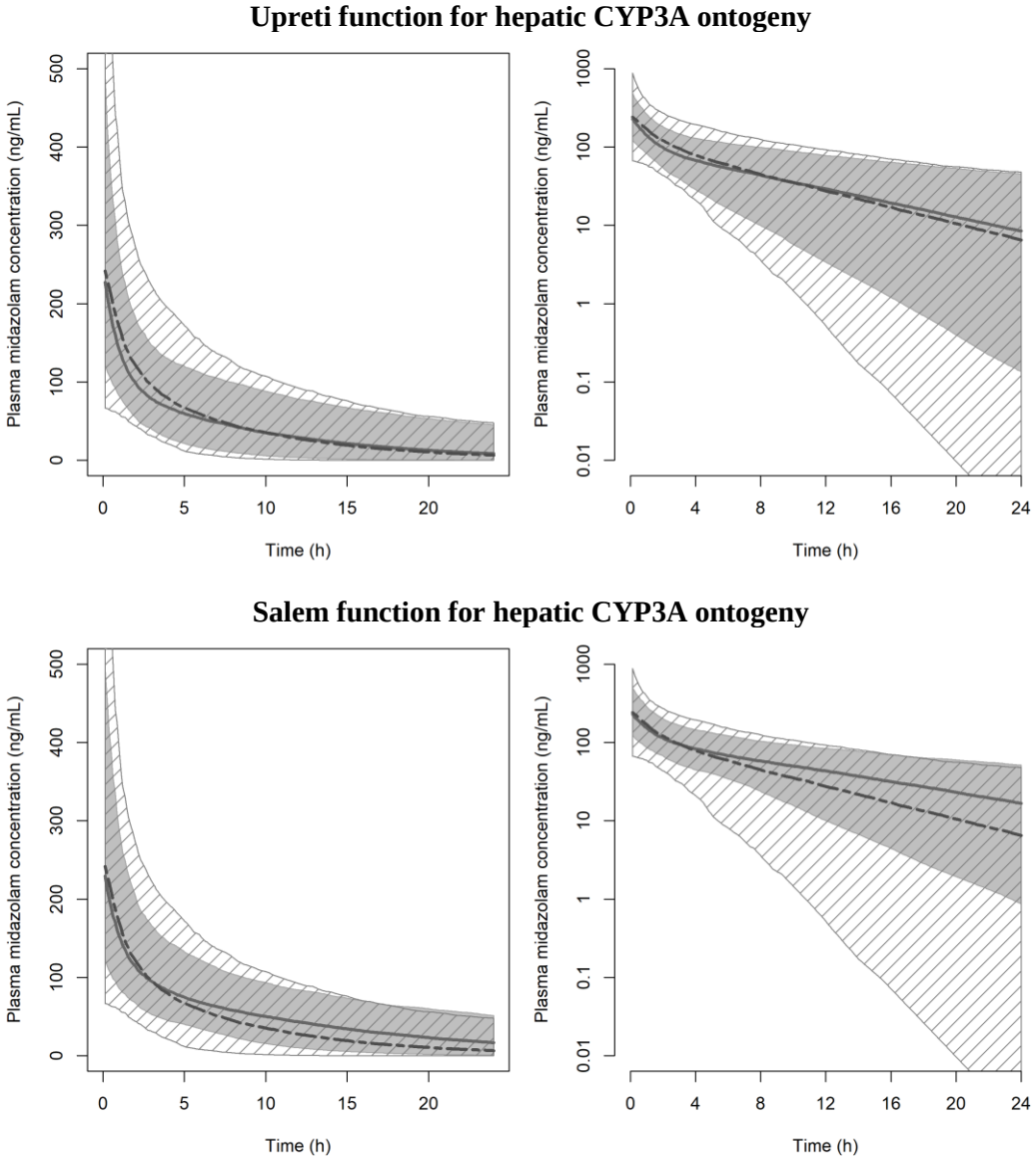

Figure S15 Comparisons of simulated plasma concentration of midazolam – time profiles after i.v. bolus administration of midazolam 0.15 mg/kg by the PBPK model and PPK model according to Burtin et al. (1994). Simulations represent the median, 5th and 95th percentiles of 1,000 virtual individuals in the age range of 0 to 10 days; simulations by the PBPK (grey shade and solid lines) and the PPK models (grey striped area and dotted lines).

The simulated plasma concentrations of midazolam by the population PK model reported by van Groen et al. (12), the median of the prediction by the PBPK model with Salem function for hepatic CYP3A ontogeny showed a good agreement in the terminal phase (Figure S16). The PBPK model prediction using Upreti function for the hepatic CYP3A ontogeny showed good agreement with the C_{max} but under-prediction in the terminal phase. The inter-individual variability predicted by the PBPK models was generally consistent with that by the population PK model.

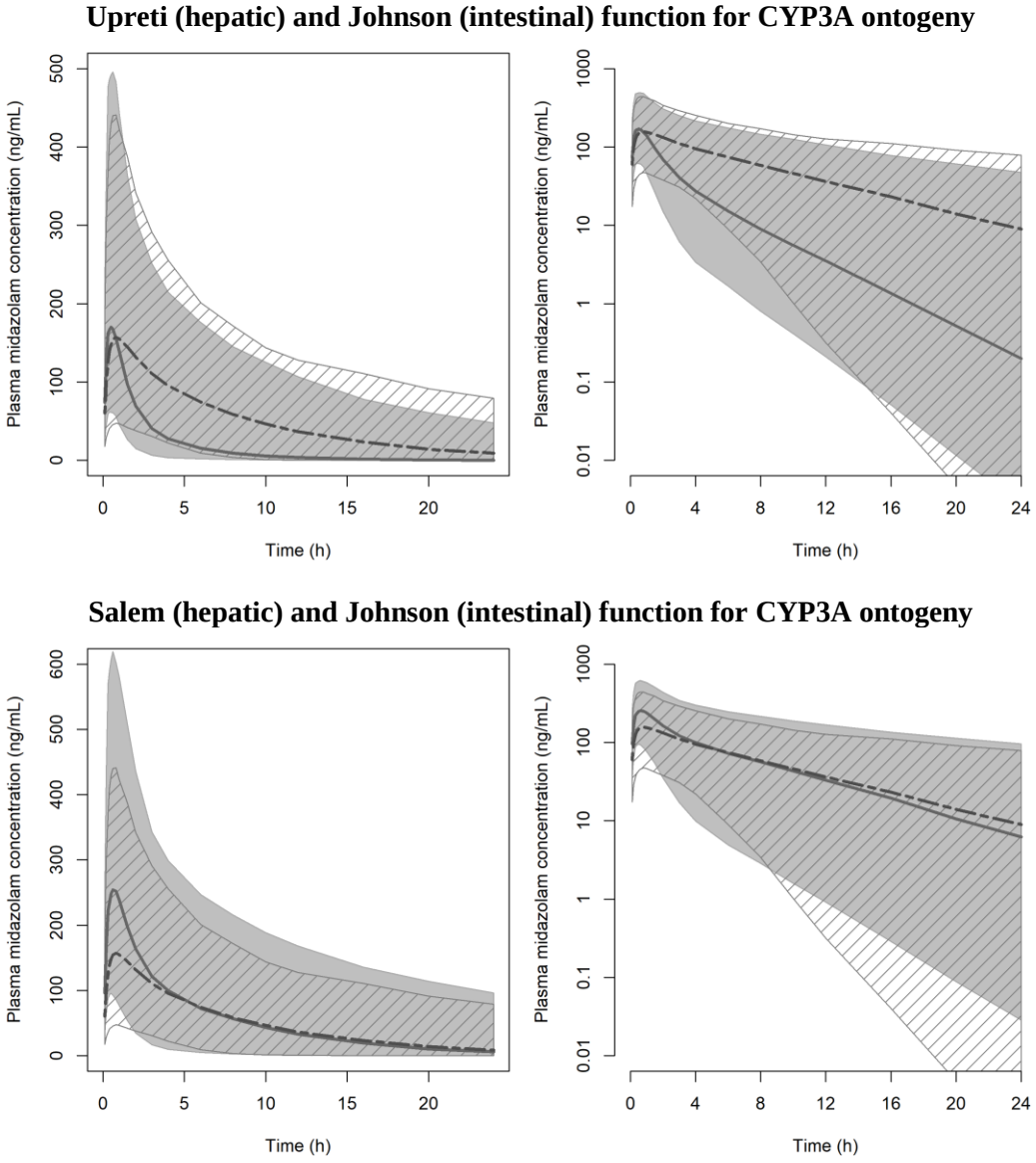

Figure S16 Comparisons of simulated midazolam plasma concentration– time profiles after an oral administration of midazolam 0.5 mg/kg by the PBPK model and PPK model according to van Groen et al. (2020). Simulations represent the median, 5th and 95th percentiles of 1,000 virtual individuals in the age range of 0.3 weeks to 5.3 years; simulations by the PBPK model (grey shade and solid lines) and PPK (grey striped area and dotted lines).

7.3 Oral bioavailability of midazolam in children

Oral bioavailability of midazolam in pediatric population was simulated using the default midazolam model and the pediatric module of Simcyp version 18. The simulation was performed for 5000 virtual pediatric population aged 0 to 12 years using Johnson function for the intestinal CYP3A ontogeny and repeated with Salem and Upreti functions for hepatic CYP3A ontogeny. Three studies reported oral bioavailability of children: 15 preterm neonates aged 3-13 days (13), 46 children aged 0.3 weeks to 5.3 years (12) and 6 children aged 6 months to 12 years (14). The simulated oral bioavailability

was compared with the observations of these studies as shown in Figure S17. The oral bioavailability of midazolam in children aged 0 to 12 years was generally well predicted by the midazolam model using Salem and Johnson functions for the hepatic and intestinal CYP3A ontogenies, respectively (Figure S17A) whereas a trend of under-prediction was noted for the model with Upreti and Johnson functions for the hepatic and intestinal CYP3A ontogenies (Figure S17B). When midazolam oral bioavailability was simulated assuming Upreti and full-maturity functions for the hepatic and intestinal CYP3A ontogenies, respectively, the extent of under-prediction was further increased (Figure S18).

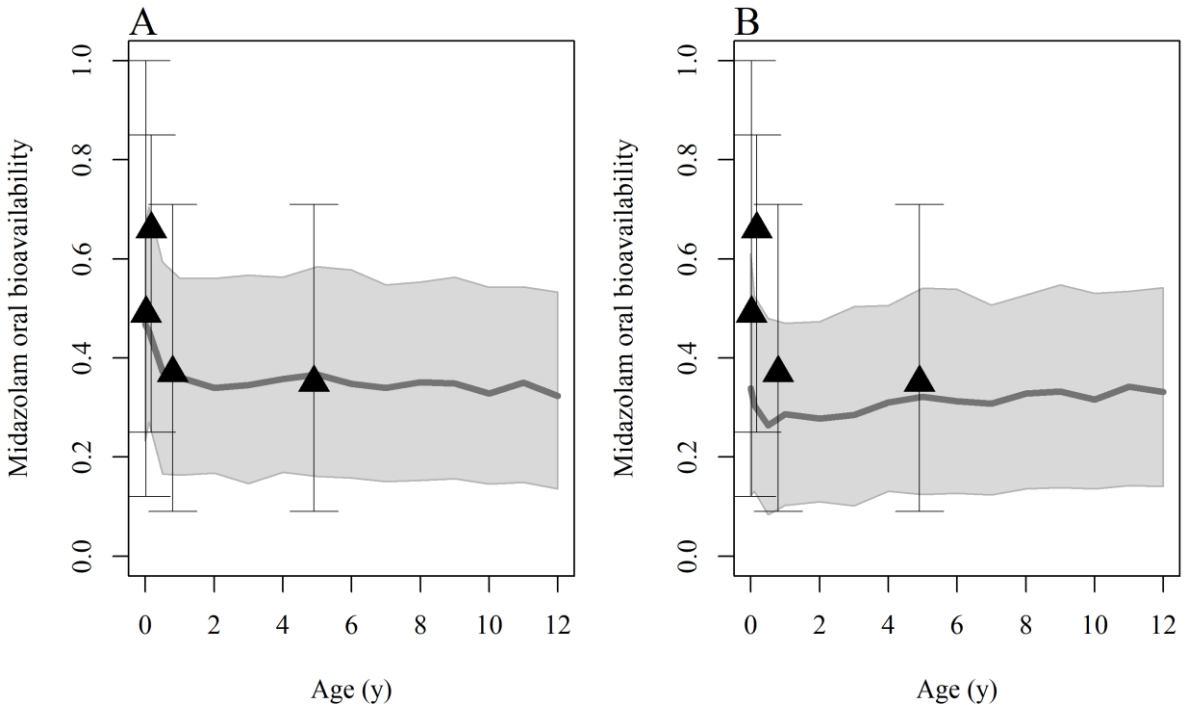

Figure S17 Predicted and observed midazolam oral bioavailability (F) in children aged 0 to 12 years using the Simcyp version 18. Median and 5th to 95th percentile of the simulated midazolam F is shown with the solid grey line and the shades. Simulations were based on Salem (A) and Upreti (B) functions for hepatic CYP3A ontogeny. Johnson function was used for intestinal CYP3A ontogeny for both simulations. The solid black triangles indicate the observed midazolam F according to de Wildt et al. (13), van Groen et al. (12) and Reed et al. (14). The whiskers indicate the range. Since Reed et al. reported the range of midazolam F for all patients 0.5-12 years, the same range is shown to the F for 0.5-2 years and 2-12 years. The median of predicted F are all within 0.8-1.25 fold of the observations except for van Groen (0.71) in A, whereas those in B are all <0.8 (0.51-0.71) except for 2-12 years by Reed et al (0.89).

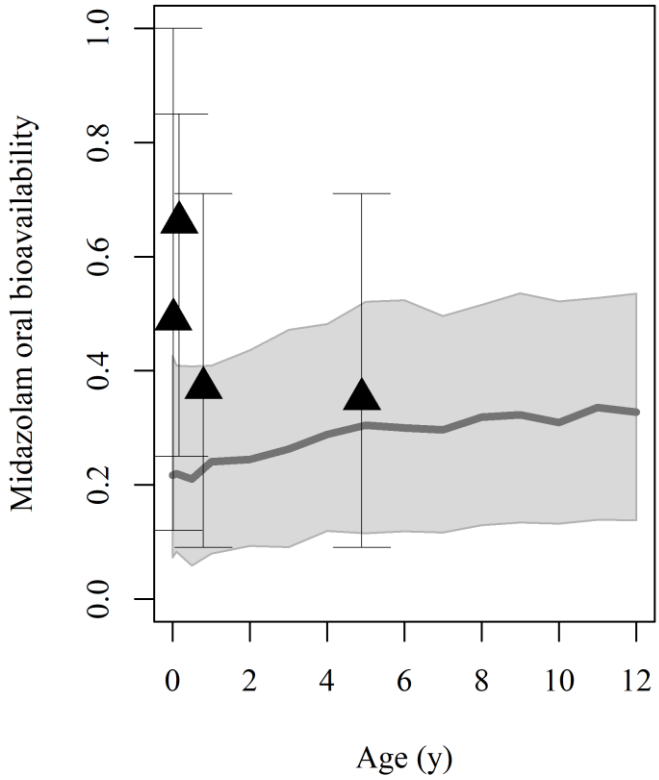

Figure S18 Predicted and observed midazolam oral bioavailability (F) in children aged 0 to 12 years using the Simcyp version 18 and Upreti function for the hepatic CYP3A ontogeny and full maturity for the intestinal CYP3A ontogeny. Median and 5th to 95th percentile of the simulated midazolam F is shown with the solid grey line and the shades. The solid black triangles indicate the observed midazolam F according to de Wildt et al. (13), van Groen et al. (12) and Reed et al. (14). The whiskers indicate the range. Since Reed et al. reported the range of midazolam F for all patients 0.5-12 years, the same range is shown to the F for 0.5-2 years and 2-12 years. The median of predicted F are all <0.8 (0.33-0.57) of the observations except for 2-12 years by Reed et al (0.82).

8. Q_{gut} model to predict the effect of risdiplam on F_G of various CYP3A substrates given orally

The Q_{gut} model (Equation S5, (15, 16)) was applied to predict the effect of risdiplam on F_G of other, more sensitive intestinal CYP3A substrates.

$$F_G = Q_{gut} /[Q_{gut} + fu_{gut} \times CL_{int,Gut}] \text{Equation S5}$$

where Q_{gut} (hybrid parameter of permeability CL and blood flow in enterocytes), fu_{gut} (unbound fraction in enterocytes) and $CL_{int,Gut}$ (intrinsic CL in the gut).

For a compound which undergoes extensive intestinal extraction (i.e., where $CL_{int,Gut} \rightarrow \infty$ and $F_G \rightarrow 0$) the equation simplifies to $F_G = Q_{gut} /[fu_{gut} \times CL_{int,Gut}]$ and therefore the F_G ratio is defined as: $F_GR = F_G' / F_G = CL_{int,Gut}/((1-x)*CL_{int,Gut})$, where *x* is the fraction of intestinal CYP3A inhibited by the TDI. Therefore, a 20% reduction in $CL_{int,Gut}$ due to the decreased intestinal CYP3A activity following risdiplam treatment would result in an 25% increase in F_G and oral AUC. It also demonstrates that the maximal extent of the intestinal contribution to oral DDI is not dependent on the F_G value of the victim drug but only the degree of inactivation by the TDI. However, the ability to estimate *x* accurately may well depend on the F_G value (sensitivity) of the probe substrate used.

9. Ontogeny functions for UGT1A4 and the theoretical AUCR of midazolam

Two UGT1A4 ontogeny functions were considered in the theoretical AUCR of midazolam: steep development over age (as implemented in Simcyp v 18) and shallow ontogeny (Simcyp version 17), as shown in Figure S19A. These ontogeny functions were compared to the Salem and Upreti functions for the hepatic CYP3A ontogeny (Figure S19B and C). The influence of UGT1A4 ontogeny functions on the DDI predictions with potent CYP3A inhibitors was examined by comparing the theoretical AUCR of midazolam according to Equation 3 in 5000 virtual pediatric population aged 0.01 – 18 years between these UGT1A4 ontogeny functions. For CYP3A ontogeny, Salem and Upreti functions were used for the liver and Johnson function was used for the intestine. The theoretical AUCR of midazolam using steep and shallow ontogeny function for UGT1A4 are shown in Figure S20A (the same as Figure 4A) and Figure S20B, respectively.

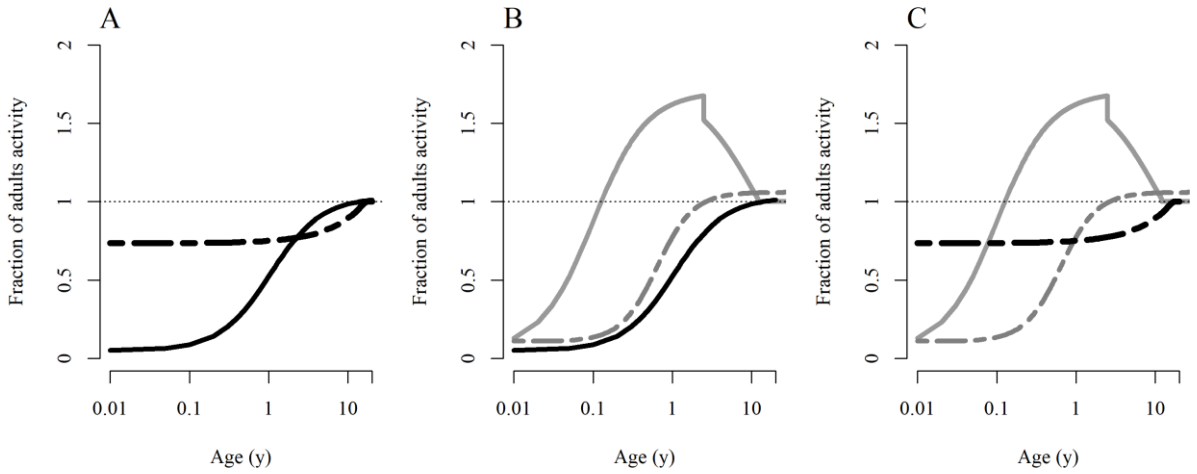

Figure S19 Comparison of hepatic ontogeny functions for UGT1A4 and commonly used hepatic CYP3A ontogeny functions. Hepatic UGT1A4 activity following steep development over age (solid black line) vs shallow (dotted black line) ontogeny function are shown (A). The steep (B) and shallow (C) hepatic UGT1A4 ontogeny functions are compared with the Upreti (grey solid line) and Salem (grey dotted line) hepatic CYP3A ontogeny functions. “Steep” and “shallow” are tentatively defined to distinguish them in the analysis.

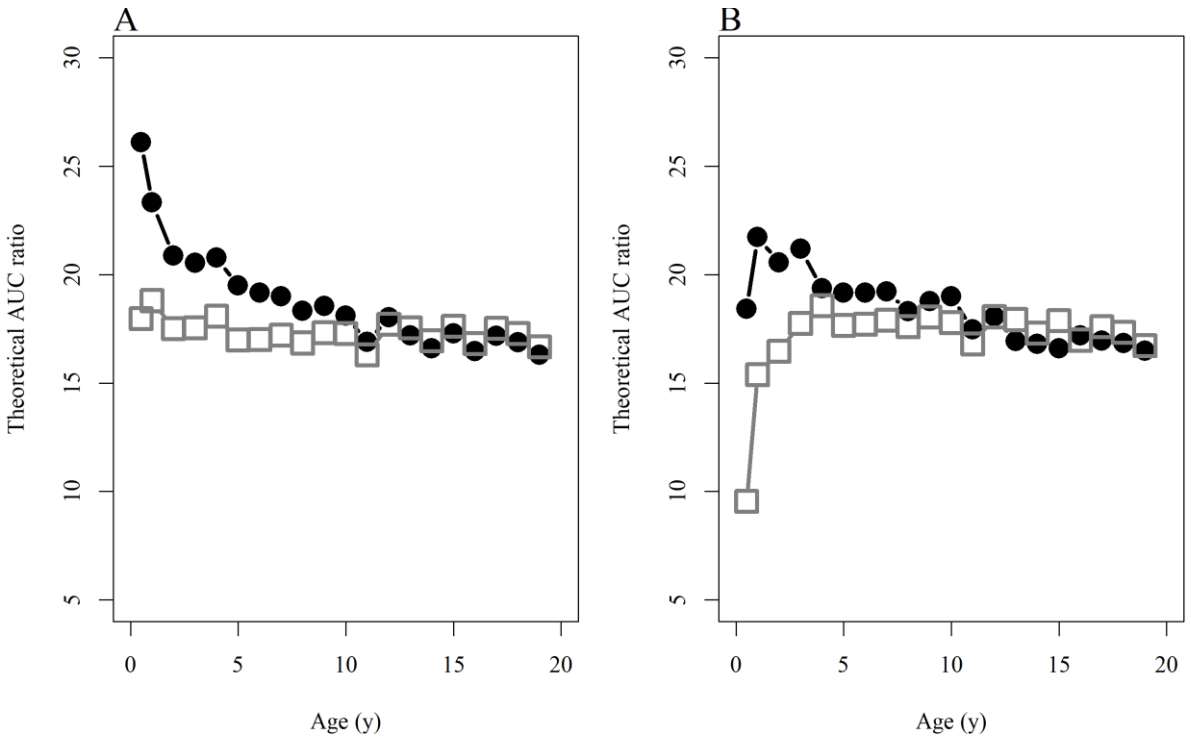

Figure S20 Predicted AUCR of midazolam in the presence of a hypothetical potent CYP3A inhibitor using either steep (A) or shallow (B) ontogeny functions for the hepatic UGT1A4 activity. The theoretical AUCR of midazolam with hepatic CYP3A ontogeny according to Salem (open squares) and Upreti (solid circles) are shown. The Johnson function was used for the intestinal CYP3A ontogeny in all simulations shown in A and B.

10. Summary of evaluation of critical input data for TDI prediction in pediatric SMA patients treated with risdiplam

Table S7 Summary of evaluations of critical input data for TDI prediction in paediatric SMA patients

Input data / assumption	Evaluation
***in vivo* TDI parameters**	• k_{inact} was informed by clinical DDI study in healthy adults at relevant risdiplam exposure in children • PPK analysis of midazolam supported the predominant effect on the first pass effect and optimization of the k_{inact} based on AUC_{last} ratio. • The worst case interpretation of k_{inact} based on C_{max} ratio was applied for the sensitivity analysis to address uncertainty of the interpretation on the TDI prediction
Age-dependent physiological data	• Hepatic (Upreti and Salem functions) and intestinal (Johnson) CYP3A ontogeny functions have adequately predicted midazolam PK in children. • The worst case intestinal CYP3A ontogeny, full maturity function, and Upreti function significantly under predicted midazolam bioavailability (F) and thus this combination of ontogeny functions represents the most conservative scenario for the TDI prediction based on current knowledge. • Uncertainty in intestinal CYP3A k_{deg} value was addressed by sensitivity analysis. The predicted TDI was insensitive to 3-fold ranges of k_{deg} values (internal data).
Intestinal concentration	• The PBPK absorption model predicted observed C_{max} well in children and adults. • The predicted almost complete absorption of risdiplam (F_A>0.9) across the age and unbound fraction in the enterocyte (fu_{Gut}) = 1 was assumed – highest possible unbound intestinal concentration • Risdiplam exhibits high permeability and no transporters are involved in the absorption process (17) • Higher intestinal concentration than healthy adults was predicted and considered for the TDI prediction in children (+82% duodenum and +31% in the jejunum).

11. References

(1) Cleary, Y., Kletzl, H., Grimsey, P., Frey, N., Silber Baumann, H., Stillhart, C., Poirier, A., Heinig, K., Fowler, S., Ogungbenro, K., Aarons, L., Galetin, A., Gertz, M. Population and physiologically-based pharmacokinetic modeling of risdiplam in infants, children and adults with spinal muscular atrophy (SMA). *ASCPT Annual Meeting 2021 CLINICAL PHARMACOLOGY & THERAPEUTICS* **VOLUME 109 S1**, (2021).

(2) Jamei, M., Dickinson, G.L. & Rostami-Hodjegan, A. A framework for assessing inter-individual variability in pharmacokinetics using virtual human populations and integrating general knowledge of physical chemistry, biology, anatomy, physiology and genetics: A tale of 'bottom-up' vs 'top-down' recognition of covariates. *Drug Metab Pharmacokinet* **24**, 53-75 (2009).

(3) Jolicoeur, P., Pontier, J., Pernin, M.O. & Sempe, M. A lifetime asymptotic growth curve for human height. *Biometrics* **44**, 995-1003 (1988).

(4) Hallifax, D. & Houston, J.B. Evaluation of hepatic clearance prediction using in vitro data: emphasis on fraction unbound in plasma and drug ionisation using a database of 107 drugs. *J Pharm Sci* **101**, 2645-52 (2012).

(5) Beal, S.L. Ways to fit a PK model with some data below the quantification limit. *J Pharmacokinet Pharmacodyn* **28**, 481-504 (2001).

(6) Williams, J.A. *et al.* Comparative metabolic capabilities of CYP3A4, CYP3A5, and CYP3A7. *Drug Metab Dispos* **30**, 883-91 (2002).

(7) Salem, F., Johnson, T.N., Abduljalil, K., Tucker, G.T. & Rostami-Hodjegan, A. A re-evaluation and validation of ontogeny functions for cytochrome P450 1A2 and 3A4 based on in vivo data. *Clin Pharmacokinet* **53**, 625-36 (2014).

(8) Upreti, V.V. & Wahlstrom, J.L. Meta-analysis of hepatic cytochrome P450 ontogeny to underwrite the prediction of pediatric pharmacokinetics using physiologically based pharmacokinetic modeling. *J Clin Pharmacol* **56**, 266-83 (2016).

(9) Smits, A., Annaert, P., Van Cruchten, S. & Allegaert, K. A Physiology-Based Pharmacokinetic Framework to Support Drug Development and Dose Precision During Therapeutic Hypothermia in Neonates. *Front Pharmacol* **11**, 587 (2020).

(10) Mulla, H., McCormack, P., Lawson, G., Firmin, R.K. & Upton, D.R. Pharmacokinetics of midazolam in neonates undergoing extracorporeal membrane oxygenation. *Anesthesiology* **99**, 275-82 (2003).

(11) Burtin, P. *et al.* Population pharmacokinetics of midazolam in neonates. *Clin Pharmacol Ther* **56**, 615-25 (1994).

(12) van Groen, B.D. *et al.* The Oral Bioavailability and Metabolism of Midazolam in Stable Critically Ill Children: A Pharmacokinetic Microtracing Study. *Clin Pharmacol Ther*, (2020).

(13) de Wildt, S.N., Kearns, G.L., Hop, W.C., Murry, D.J., Abdel-Rahman, S.M. & van den Anker, J.N. Pharmacokinetics and metabolism of oral midazolam in preterm infants. *Br J Clin Pharmacol* **53**, 390-2 (2002).

(14) Reed, M.D. *et al.* The single-dose pharmacokinetics of midazolam and its primary metabolite in pediatric patients after oral and intravenous administration. *J Clin Pharmacol* **41**, 1359-69 (2001).

(15) Yang, J., Jamei, M., Yeo, K.R., Tucker, G.T. & Rostami-Hodjegan, A. Prediction of intestinal first-pass drug metabolism. *Curr Drug Metab* **8**, 676-84 (2007).

(16) Gertz, M., Harrison, A., Houston, J.B. & Galetin, A. Prediction of human intestinal first-pass metabolism of 25 CYP3A substrates from in vitro clearance and permeability data. *Drug Metab Dispos* **38**, 1147-58 (2010).

(17) FDA, U. Center for Drug Evaluation and Reserach. Application Number: 213535Orig1s000 Clinical Pharmacology Review(s). *https://wwwaccessdatafdagov/drugsatfda_docs/nda/2020/213535Orig1s000ClinPharmRpdf* **Accessed March 2021.**, (2020).